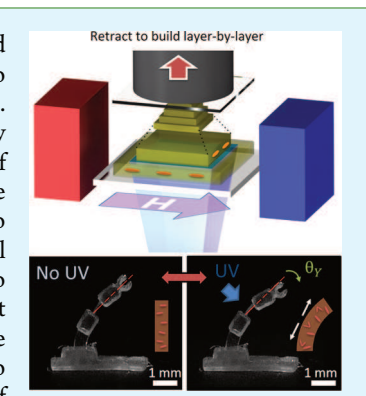


# Voxelated Molecular Patterning in Three-Dimensional Freeforms

Mohsen Tabrizi, † Taylor H. Ware, † and M. Ravi Shankar\*, †

Supporting Information

ABSTRACT: The ability to pattern material response, voxel by voxel, to direct actuation and manipulation in macroscopic structures can enable devices that utilize ambient stimuli to produce functional responses at length scales ranging from the micro- to the macroscopic. Fabricating liquid crystalline polymers (LCPs), where the molecular director is indexably defined in three-dimensional (3D) freeforms, can be a key enabler. Here, the combination of anisotropic magnetic susceptibility of the liquid crystalline monomers in a reorientable magnetic field and spatially selective photopolymerization using a digital micromirror device to independently define molecular orientation in light and/or heat-responsive multimaterial elements, which are additively incorporated into 3D freeforms, is exploited. This is shown to enable structural complexity across length scales in nontrivial geometries, including re-entrant shapes, which are responsive to either heat or light. A range of monomer compositions are optimized to include photoinitiators, light absorbers, and polymerization inhibitors to modulate the polymerization characteristics while simultaneously retaining the tailorability of



the nematic alignment. The versatility of this framework is illustrated in an array of examples, including (i) thermomechanical generation of Gaussian-curved structures from flat geometries, (ii) light-responsive freeform topographies, and (iii) multiresponsive manipulators, which can be powered along independent axes using heat and/or light. The ability to integrate responses to multiple stimuli, where the principal directions of the mechanical output are arbitrarily tailored in a 3D freeform, enables new design spaces in soft robotics, micromechanical/fluidic systems, and optomechanical systems.

KEYWORDS: smart materials, liquid crystal polymers, additive manufacturing, 4D printing, soft robotics

## 1. INTRODUCTION

Regulating functional properties and directing structural evolution in active polymers by programming composition and microstructural gradients during fabrication are a versatile route for realizing soft machines. Integrating active elements with suspensory structures, including fluidic and solid and mechanical logic elements, has been used to encode macroscopic actuation and manipulation in soft robots. If individual voxels of a material themselves become capable of active functionalities, a broader design space of encodable responses can emerge by blurring the distinction between the active and the suspensory, structural elements. The material itself becomes the robotic manipulator. For example, programming anisotropic magnetic domain structures in magnetic particleinfused polymeric inks can enable soft robots, which manifest nonlinear shape transformations using magnetic fields.<sup>3</sup> Biomimetic transformations have also been realized via anisotropic swelling in structures three-dimensional (3D)printed with aligned nanocellulose fibers. The underlying organizing principle is to exercise voxel-by-voxel control over both the geometry and the anisotropic coupling between a stimulus and material response. When responsiveness, geometry, and mechanics conspire, emergent design opportunities become possible.

Liquid crystalline polymers (LCPs) are distinguished among stimuli-responsive materials due to their ability to reversibly generate work densities in excess of ~I/kg with unusual forcedisplacement characteristics. Notably, the ability to simultaneously generate large strains (10's%) and actuation stresses (100's kPa) from order-disorder transitions of the long-range orientational order in the macromolecular network. 5-7 Actuation can be induced using a range of stimuli, including heat, light, and solvent. 8,9 Therefore, the untethered LCP smart structures can be activated remotely using, say, ambient energy without being encumbered by on-board power sources (e.g., batteries). Light is a particularly attractive energy source for driving mechanical adaptation, where it can selectively address actuation with spatiotemporal selectivity at length scales ranging from the micro- to the macroscopic scales. Typically, principal directions of actuation strains are derived from the anisotropy of the molecular directorcontractile strains are generated parallel to the director, and tensile strains emerge perpendicular to it. 10 Blueprinting spatially heterogeneous molecular patterns to direct the large work potential is a compelling feature of the LCP. This allows

Received: March 13, 2019 Accepted: July 16, 2019 Published: July 16, 2019

Department of Industrial Engineering, Swanson School of Engineering, University of Pittsburgh, Pittsburgh, Pennsylvania 15261, United States

<sup>&</sup>lt;sup>‡</sup>Department of Bioengineering, The University of Texas at Dallas, Richardson, Texas 75080, United States

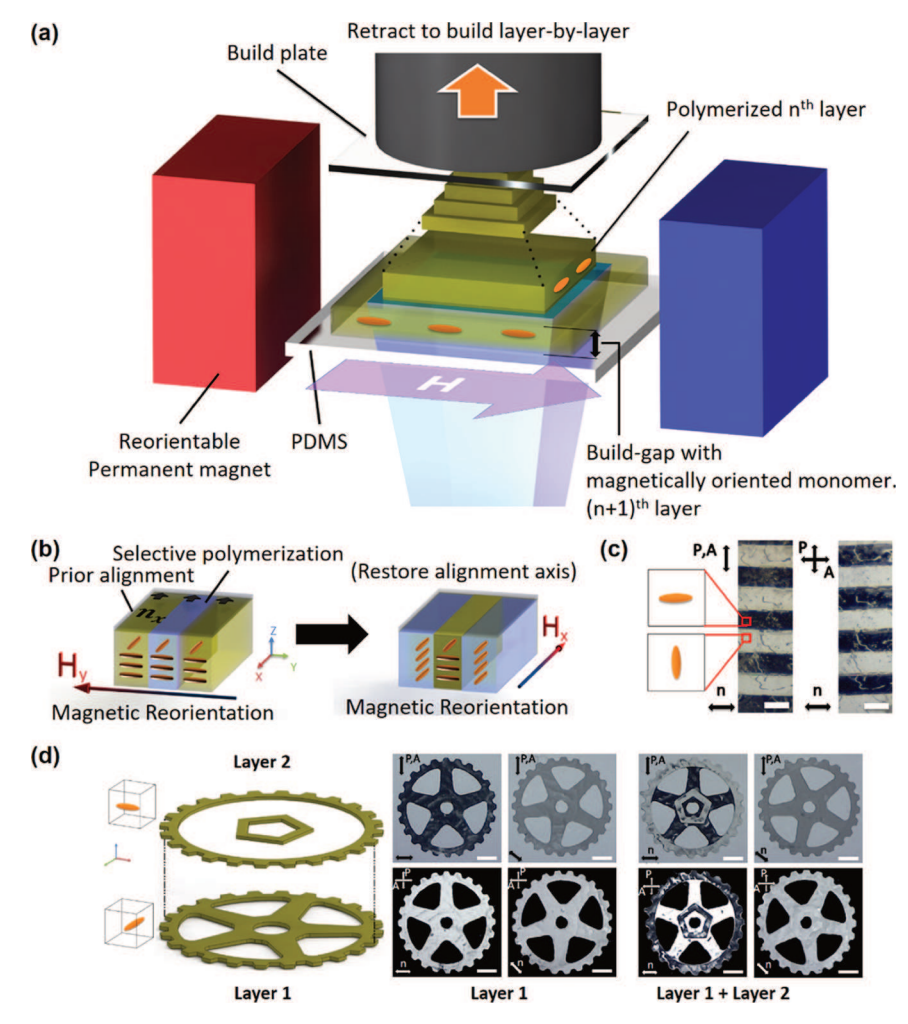


Figure 1. (a) Schematic of a layer-by-layer 3D printing system capable of fabricating three-dimensional geometries with molecular alignment encoded using a magnetic field. Reorienting the magnetic field on demand and spatially selective polymerization using a DMD light source allow for independently indexing the molecular orientation voxel by voxel. See Supporting Information, Figure S1 for an illustration of the physical setup. (b) Example of control over the molecular director within a given layer. A build plate with an alignment layer is used to trigger a preferred alignment direction. Application of a magnetic field reorients this alignment, which is selectively frozen in via cross-linking. Then, the magnetic field is rotated to coincide with the prior orientation, following which cross-linking is used to preserve the patterning. (c) Polarized optical microscopy (POM) images of the sample with mutually orthogonal molecular orientation, which was generated using the steps described in (b). The regions with a uniaxial alignment are bright (maximum light transmission through the material, polarizer, and analyzer) at 0° and dark (less light transmission) at 45° under parallel polarizers (images in the left) and dark at 0° and bright at 45° under crossed polarizers (images in the right). Other regions are characterized by a pattern, which is rotated through the thickness. (d) Ability to pattern arbitrary features, while achieving molecular alignment is illustrated by printing a bilayered gear-shaped structure. The exploded view of the structure and the director orientation for each layer is shown. The build plate, similar to (b) and (c), is composed of a rubbed elvamide layer, which enforces a preferred orientation. The first layer is created by applying a magnetic field orthogonal to this orientation, which leads to a rotation of the director. The second layer, which consists of the hub and teeth of the gear, is rotated with respect to the first layer to reset the alignment with respect to the rubbing direction on the build plate. The images on the right are POM images of the first layer and the final bilayer structure at 0 and 45° under parallel and crossed polarizer (P) and analyzer (A), respectively (all scale bars = 1 mm).

for their utilization in actuators across length scales ranging from the micrometer to the macroscopic scale. <sup>11–13</sup> Furthermore, exploiting the competition between bending/stretching in slender objects allows for eliciting the rare combination of high-force/large-displacement actuation from hitherto small form-factor actuators. <sup>13</sup>

Blueprinting molecular patterns has often relied on liquid crystalline (LC) self-assembly of the monomers, which is frozen in by cross-linking to create the LCP, often via photopolymerization. Utilizing command surfaces, which have themselves been patterned mechanically, optically, or topographically, an array of LCP director patterns can be generated. Utilization of anisotropic magnetic fields to drive

alignment has resulted in two-dimensional (2D)<sup>14</sup> or 2.5-dimensional<sup>15</sup> geometries polymerized in molds, although the ability to build 3D freeforms with arbitrarily voxelated LC ordering remains elusive. Harkening back to Finkelmann's method for driving alignment via mechanical stretching followed by cross-linking,<sup>6</sup> extrusion-based methods have been pursued for the additive fabrication of LCP.<sup>16–21</sup> Shear imposed on oligomeric inks during extrusion orients the nematic director along the print direction, which is optically cross-linked, soon after the deposition. The raster pattern, which is defined during the build sequence, determines the director field during the fabrication of macroscopic geometries.<sup>16–21</sup>

Table 1. Heat-Responsive Monomer Mixtures of Various Compositions, Their Curing Temperature, and Parameters

	monomer			
chemical composition and printing process conditions	R3P1T1	R3P0.5T1	R3P1T4	R3P1T1I0.5
RM257 [wt %]	98	98.5	95	97.5
Azo 6C [wt %]	0	0	0	0
I369 photoinitiator [wt %]	1	0.5	1	1
I784 photoinitiator [wt %]	0	0	0	0
Tinuvin (UV light absorber) [wt %]	1	1	4	1
methyl red (visible light absorber) [wt %]	0	0	0	0
inhibitor methylhydroquinone [wt %]	0	0	0	0.5
curing temperature [°C]	100	100	100	100
$Q_c [mJ/cm^3]$	$20.8 \pm 3.1$	$66.0 \pm 2.2$	$44.1 \pm 5$	$105.3 \pm 2.6$
$D_0 \ [\mu \mathrm{m}]$	$909 \pm 105$	$1083 \pm 80$	$740 \pm 116$	$352 \pm 50$

Exploiting the full potential of LCP in adaptive structures and mechanisms requires an ability to define the molecular orientation, voxel by voxel, during the fabrication of a 3D freeform. Doing so holds the key to encoding arbitrary transformations of three-dimensional geometries along with predefined target metrics,<sup>22</sup> which is defined for each voxel. This unlocks a pathway for designing transformable 3D geometries, including complex active kinematic and mechanical logic units, biomimicking actuators, and harnessing magnified actuation profiles in soft robotics. Current fabrication approaches constrain the ability to access this 3D design space. The command surface-based methods are intrinsically limited to flat geometries (typically films of <100  $\mu$ m), necessitating lamination-based assembly for scaling the responsiveness.<sup>23</sup> Although researchers have utilized the direct laser writing (DLW) method through a two-photon polymerization of the LCP monomers to make complex microscale structures, the molecular orientation imposed by the surface is the same for the whole structure. 24,25 While freeforms can be created, they lack the ability to voxelate the stimuli response with indexable, spatial selectivity within the structure. Fabrication in molds limits geometries to those that can be reliably extracted following polymerization. 14,15 Depositionbased methods can generate arbitrary geometries but cannot decouple molecular patterning from the build sequence. 16-21 Contrast deposition-based methods against an approach, where the molecular orientation can be independently defined with, say, 1° resolution per 50  $\mu$ m element. For a 1 mm segment, the latter method offers a design space, which is larger by a factor of  $\sim 10^{40}$  in comparison to the depositionbased method. Assuming that 180° is available with 1° resolution per 50 µm length, the total number of design permutations is  $180^{(1000/50)} \approx 10^{40}$ . For a 1 mm<sup>3</sup> volume, the design space is larger by a googol.

Here, we present a framework for breaking out of the confines of prior approaches by exploiting the combination of anisotropic magnetic susceptibility of the LC monomers and spatially selective photopolymerization using a digital micromirror device (DMD) in a bottom-up (inverted) 3D printing configuration. The system illustrated in Figure 1a (see also Figure S1, Supporting Information) utilizes an indexable 300 mT magnetic field (H) generated using permanent magnets, which are mounted on a rotation stage to drive the alignment of the LC monomers. A DMD system (Vivitek D912HD projector) with a pixel resolution of  $\sim 50 \mu m$  polymerizes desired regions to preserve this orientation with spatial selectivity. This method has salient advantages in comparison to traditional, command surface-induced alignment. Typically,

molecular ordering is limited to within tens of micrometer of the command surface. 5,26,27 Using a magnetic field, however, influences the alignment within the bulk of the nematogenic monomer, where the selective polymerization can freeze the alignment, as desired. This can simultaneously offer scalability of the fabrication from the micro- to the macroscale while preserving the spatial resolution of the individual voxels. The dimensions of the voxels are defined by the resolution of the DMD system (tens of micrometers). The magnetically assisted alignment is capable of encoding each voxel independent of the geometry. Independently dictating the alignment using a reorientable magnetic field and polymerizing as needed to build a 3D freeform layer by layer allows for fabricating structures, where the molecular alignment and the geometry can be defined in a truly voxel-by-voxel fashion. Furthermore, during the fabrication of each layer, the monomer is confined in a build gap between the priorly polymerized layer (or the build plate, if it is the first layer) and a polydimethylsiloxane (PDMS) substrate. After selective polymerization under the influence of the reorientable magnetic field, the polymerized layer is detached from the PDMS substrate by retracting the build plate to create the subsequent build gap. The sample remains attached to the build plate during the build process, and after each retraction of the build plate, a fresh monomer mixture (of same or different composition) is introduced. The process is then repeated. Thus, we decouple the endowment of molecular alignment (defined by the field orientation) from the material build path (defined by the DMD system). As a result, the molecular orientation that was previously constrained by the geometry and the surface patterning or command layers can now be directly encoded. Designing geometries from responsive materials allows for exploiting mechanical nonlinearities. These include snap-through instabilities, 28 supercoiling phenomena 29 and related torsional instabilities,<sup>30</sup> and bucklings of plates.<sup>31</sup> This opens the door for realizing ms-scale actuation profiles in soft actuators while simultaneously eliciting multiaxial actuation. This framework also allows for arbitrary modulation of the composition of the material from one layer to another. Functional gradations become possible to integrate multiresponsiveness in a facile manner to create response profiles, which were hitherto

Building LCP in this fashion encounters a constraint where a given voxel or a layer influences the patterning in a neighboring element, which is subsequently built. Consider the example of a multilayered geometry in Figure 1a, where layer n has an orientation, which is transverse to that in the monomer in the build gap below it. The monomer will eventually become layer

controlled voxel by voxel.

n + 1 with an orientation determined by the magnetic field. The spatial extent to which the alignment in the layer n + 1 will be influenced by the anchoring from layer n will determine the finest resolution capable with this platform. This is essentially parameterized by De Gennes's magnetic coherence length  $(\xi)$ , which for a 300 mT magnetic field is  $\xi = \frac{1}{H} \sqrt{\frac{K_{22}}{\chi_a}} \ll 10 \,\mu m$ , assuming  $K_{22} \sim 10^{-7}$  dyne (twist Frank constant) and  $\chi_a \sim 10^{-7}$  (the anisotropy of magnetic susceptibility in c.g.s.).  $^{32,33}$  In a typical voxel 50  $\mu$ m  $\times$  50  $\mu$ m  $\times$  50  $\mu$ m, when the characteristic dimensions are much larger than  $\xi$ , the effect of anchoring from adjacent voxels declines exponentially and the alignment will be essentially dictated by the magnetic field.<sup>3</sup> Hence, for the resolutions targeted here, this platform becomes

viable for the layer-by-layer fabrication of molecularly ordered

freeforms, where within each layer, the director can be

This platform does not restrict the molecular director to a fixed orientation in a given layer. Figure 1b illustrates the creation of multiple nematic orientations in different voxels of a single layer. To demonstrate the idea, a glass build plate was spin-coated with Elvamide (DuPont) and rubbed to create a surface-anchoring condition (along  $n_x$ ) to emulate a prior layer and it is positioned 50  $\mu$ m away from a PDMS substrate. A monomer mixture (R3P1T4 in Table 1) composed of 95 wt % mesogenic monomer RM257 (2-methyl-1,4-phenylene-bis[4-[3(acryloyloxy)propyloxy]benzoate]), 1 wt % photoinitiator Irgacure 369 (2-benzyl-2-dimethylamino-1-(4-morpholinophenyl)-butanone-1), and 4 wt % UV absorber Tinuvin 328 (2-(2H-benzotriazol-2-yl)-4,6-di-tert-pentylphenol) was introduced in the build gap. A constant temperature of 100 °C was maintained, and a 300 mT magnetic field was applied perpendicular (in plane) to the surface-anchoring direction for 300 s (dwell time). Selective photopolymerization (with a 0.8 s exposure time and 170 mW cm<sup>-2</sup> intensity) using the DMD system was used to cross-link regions with a director pattern, which is rotated by  $\pi/2$  with respect to the prior alignment. After which the magnetic field was rotated to restore the axis with  $n_x$  in the unpolymerized regions. Meanwhile, the alignment of the already cross-linked regions remains fixed. Cross-linking of the remaining monomer was then used to generate a striped sample with alternating layers of uniform alignment along  $n_x$  in some regions and rotated nematic patterns in the rest. Figure 1c illustrates the polarized optical microscopy (POM) images of a single layer built using this idea. The parallel and crossed polarizer (P) and analyzer (A) images illustrate regions where the director patterns are all aligned along  $n_x$  or are rotated perpendicular with respect to  $n_x$ by the magnetic field.

At this point, it becomes possible to marry spatially selective polymerization with spatially resolved blueprinting of the director patterns to build geometries layer by layer. Figure 1d illustrates a two-layered gear-shaped structure. Here, the first layer is characterized by the planar orientation of the nematic director (perpendicular to the rubbing direction), where the corresponding geometric profile is selectively built. Then, the built plate is raised, the monomer is introduced into the build gap, and the magnetic field is oriented transverse to this orientation. Then, the teeth and the hub are selectively polymerized with the rotated orientation. The POM images were recorded after the first layer was built and after both layers were created. Figure 1d illustrates images with both

crossed polarizers (polarizer P perpendicular to analyzer A) and with P parallel to A for each case.

Parenthetically, we note the presence of a temperature window for orienting and polymerizing the mesogenic monomers without requiring any temperature cycling. The ability to 3D-print molecularly ordered polymers at a constant temperature eliminates in-process deformation of the responsive material and added process time due to the heatingcooling cycles. Often, temperature cycling into the isotropic state of the monomer followed by cooling into the nematic state in the presence of an orienting field has been used. 15,34 Eliminating this thermal cycling decreases the possibility of thermal curing of the monomer during printing.

### 2. RESULTS AND DISCUSSION

When seeking to create complex geometries with highly defined structural features, the ability to control the polymerization depth in individual polymerized voxels becomes critical. We find that the interplay of the optical absorption of absorbing dyes and relative concentrations of photoinitiator and inhibitor of polymerization provides control over the depth to which cross-linking occurs within the build gap. However, for this control, as the material is built, unintended polymerization can occur, especially when overhanging structures are fabricated in subsequent layers. To achieve this control, while simultaneously achieving molecularly ordered LCP, a range of monomer mixtures were developed. RM257, a diacrylate, was used as the host mesogen, which generate temperature-sensitive actuation. Doping with an azobenzenefunctionalized cross-linker (Azo 6c) endows light-responsive actuation. Details can be found in the experimental section. For the compositions shown in Tables 1 and 2, the

Table 2. Light-Responsive Monomer Mixtures of Various Compositions, Their Curing Temperature, and Parameters

	monomer	
chemical composition and printing process conditions	RZ7P1	RZ7P1R0.1
RM257 [wt %]	89	88.9
Azo 6C [wt %]	10	10
I369 photoinitiator [wt %]	0	0
I784 photoinitiator [wt %]	1	1
Tinuvin (UV light absorber) [wt %]	0	0
methyl red (visible light absorber) [wt %]	0	0.1
inhibitor methylhydroquinone [wt %]	0	0
curing temperature [°C]	95	95
$Q_c [mJ/cm^3]$	$194.6 \pm 23.1$	$565.1 \pm 24.4$
$D_0$ [ $\mu$ m]	$628 \pm 56$	$113 \pm 6$

polymerization depth  $(D_p)$  is found to be a function of the photonic energy dosage ( $\sim It$ ), where I is the intensity and t is the exposure time. We utilize the scaling relation:  $D_p = D_0$  $\ln(It/Q_c)$ , where  $D_0$  and  $Q_c$  are constants characteristic of the monomer mixture. <sup>35</sup> Figure 2a illustrates the "working curves" for the various compositions in Tables 1 and 2.  $D_0$  encapsulates the effect of attenuation of light through the monomer and its effect on the depth to which polymerization occurs. An effective approach for controlling this parameter is via the addition of the absorbing dyes. For thermally responsive RM257-based resins (Table 1), controlling the concentration of the UV absorber (Tinuvin) leads to a smaller  $D_0$ . See Figure 2a for comparison of R3P1T1 vs R3P1T4, where the slope of

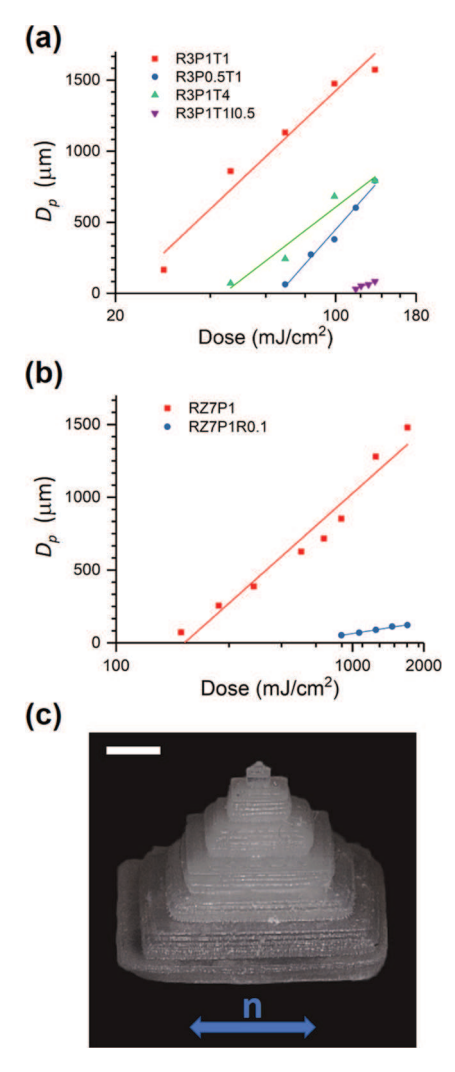


Figure 2. Polymerization depth as a function of irradiation energy dosage for various compositions. (a) Heat-responsive LCP mixtures. (b) Azobenzene-functionalized light-responsive mixtures. (c) Image of a 3.8 mm high pyramid structure made of R3P1T1 which is aligned uniaxially (blue arrow) throughout the sample. This figure illustrates the scalability of the proposed fabrication method (scale bar = 1 mm).

the working curve is smaller with increasing UV absorber. The effect of the photoinitiator on the slope, however, is small as seen from the comparison of R3P1T1 vs R3P0.5T1. These systems are polymerized using Irgacure 369 (Ciba) as the photoinitiator and using unfiltered irradiation from the projector, which has components from UV to visible. In contrast, the azobenzene-functionalized materials (Table 2) are polymerized using light filtered with a 495 nm long-pass filter to avoid isomerizing the azobenzene during the polymerization. Here, Irgacure 784 (Ciba) is used as the photoinitiator and methyl red is used as the absorber. The working curves for the photoresponsive resins are illustrated in Figure 2b. We identify compositions and processing conditions to overcome challenges in the incorporation of photochromic molecules, which modify the stability of the mesophase and present challenges in cross-linking monomers with spatial selectivity to preserve the molecular order.  $^{36,37}$  The constant  $Q_c$  in Figure 2a,b is correlated with the minimum energy density that is required to start the polymerization, which increases when the amount of photoinitiator is decreased. This can be seen by

comparing Q<sub>c</sub> for R3P1T1 vs R3P0.5T1. A similar increase in the  $Q_c$  is observed when a polymerization inhibitor (methylhydroquinone) is added in the composition R3P1T1I0.5. Increasing  $Q_c$  leads to a shifting of the working curves to the right, wherein the intercept along the x-axis (energy dose) increases. These calibration curves enable the scalable fabrication of molecularly ordered freeforms at scales, which outstrip conventional cell-based fabrication methods, while also enabling precise control over the geometry. Figure 2c illustrates a pyramid-like structure fabricated with R3P1T1, where the molecular director (n) throughout the sample is oriented along the indicated arrow. The pyramid is 3.8 mm high made of 38 layers with a 100  $\mu$ m layer thickness. Access to molecularly patterned structures at these scales holds the key to magnifying the work potential and the utility of LCP actuators in practical systems.

The ability to fabricate molecularly ordered freeforms allows for harnessing nonlinear mechanics to enable new pathways for shape selection. Consider a bilayered flat strip structure printed using R3P1T1 in Figure 3a, where a uniformly oriented monodomain sample of 50  $\mu m$  in thickness resides on a randomly oriented substrate of 50  $\mu$ m thickness. The monodomain sample is created by polymerizing the strip under a stationary magnetic field, while the random polydomain portion is created by polymerizing in the absence of a magnetic field. The width of the sample in the third dimension is 0.5 mm. The monodomain portion will respond by shrinking along the long axis, while the polydomain sample produces no net strain. As a result, heating the sample leads to a curvature of the bilayer ( $\kappa = 0.98 \text{ mm}^{-1}$ ), as illustrated. The ability to directly fabricate complex geometries to exploit mechanical nonlinearities that elicit unusual shape transformations, a bilayer basket-shaped configuration, was printed. Here, a ring-shaped structure was printed, segment by segment (see Figure S2), with the director pattern, which is azimuthally oriented. This ring can also be thought of as an annular section of a +1 topological defect. 13 This was integrated with a subsequent layer, which was printed with a square weavehatched pattern and a polydomain alignment, in the absence of a magnetic field.

This structure allows for exploiting the idea of overcurvature to create geometries with a Gaussian curvature, even when starting from a prior flat state.<sup>38</sup> While a bilayered flat strip will bend when heated, confining the bilayer into a closed ring with a curvature orthogonal to that generated with heat can trigger buckling out of the plane. While this has been explored in the buckling of rods,<sup>38</sup> here, we exploit our fabrication platform to drive transformations of surfaces from a flat state into the one characterized by negative Gaussian curvature. The overcurvature is defined by the parameter  $O_p = \sqrt{1 + (\kappa R)^2}$ , where  $\kappa$  is the curvature caused by the heat actuation (same as the curvature of the flat bilayered strip after heating) and is orthogonal to the in-plane curvature  $R^{-1.38}$  At room temperature  $O_p = 1$  ( $\kappa = 0$ ), the geometry is flat with an initial curvature  $R^{-1}$ . R = 2.6 mm in Figure 3a. By increasing the temperature  $(\kappa > 0)$ , the ring generates an orthogonal curvature  $\kappa$ . As the periphery of the sample buckles out of plane to minimize the bending and torsional energies, the hatched surface is forced by the constraints along its periphery into a negative Gaussian-curved shape. By modifying the value of R, differing levels of overcurvature can be accessed to create

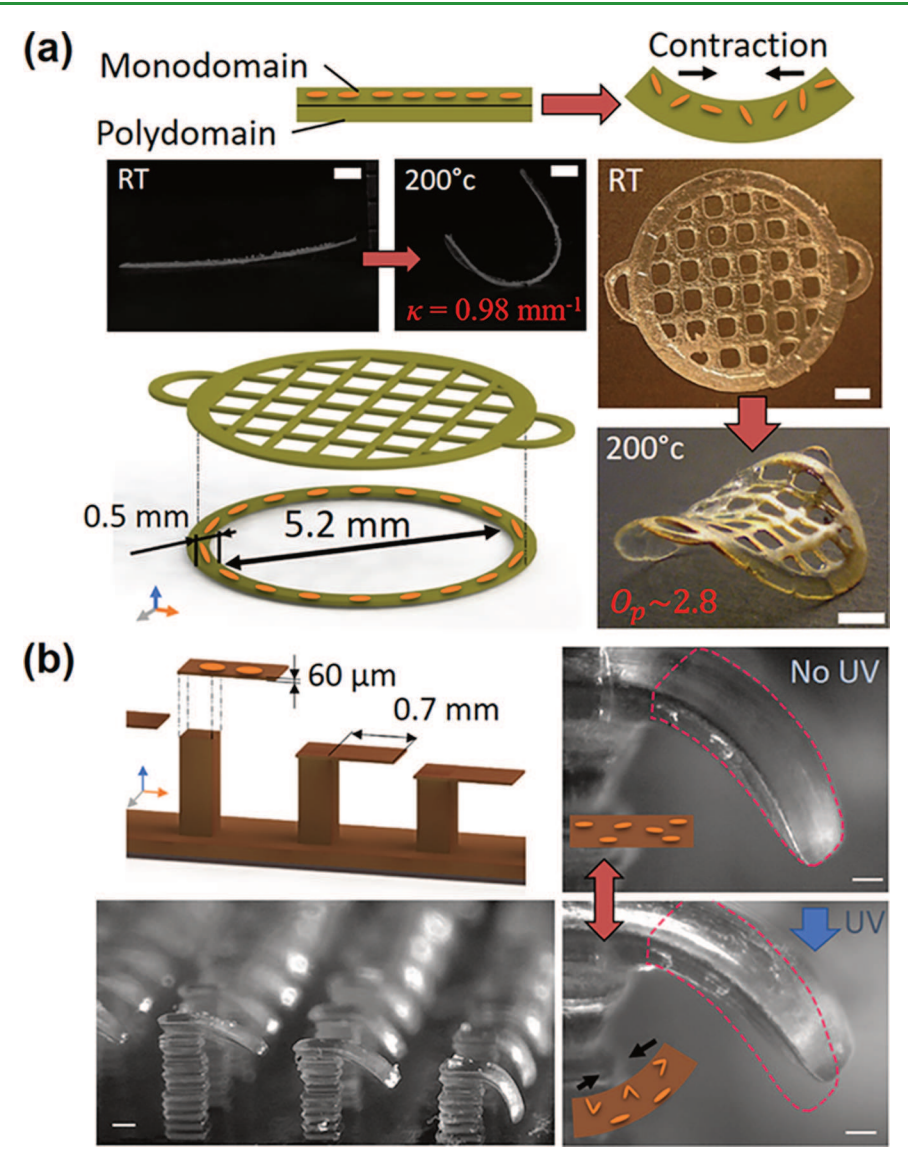


**Figure 3.** (a) Harnessing the response of a 3D-printed bilayered actuator in the overcurvature-driven assembly of Gaussian-curved geometries in R3P1T1. A strip composed of a uniformly oriented LCP residing on a polydomain LCP (printed without applying a magnetic field) generates a curvature ( $\kappa$ ) when stimulated with heat. However, creating an annular geometry with an azimuthally patterned director, which resides on a hatch-patterned suspensory structure (polydomain), elicits the creation of a Gaussian-curved (saddle-like geometry), when heated (scale bars = 1 mm). The exploded view of the hitherto flat geometry, before heating, is also illustrated. (b) Light-responsive array of microstructures fabricated with RZ7P1R0.1 is shown. The overhanging cantilevers are monodomain, while the vertical pillars are polydomain. Irradiation with 365 nm UV elicits a bending of the cantilevers. The insets illustrate the schematic of actuation due to the photoisomerization of azobenzene. Red dashed outlines indicate the initial shape of the cantilever before the actuation (scale bar of the array image = 200 μm, scale bars of a single cantilever on the right = 50 μm). Also, see SI Movie 1.

a range of geometries following thermal stimulation (see Figure S3, Supporting Information).

Monomer system RZ7P1R0.1 was used to demonstrate the fabrication of light-responsive microstructures in Figure 3b. Azobenzene-functionalized mixtures result in a glassy LCP, which respond to irradiation with 365 nm UV by bending toward the actinic light.<sup>39</sup> The ability to spatiotemporally modulate the actinic light to direct actuation in microstructures is particularly attractive for creating functional surfaces and active topographies. In contrast to prior approaches, involving cholesteric self-assembly or micromolding, <sup>11</sup> the design space possible with the 3D printing approach is broader, including opportunities creating re-entrant microstructures, which are capable of unusual properties (e.g., robust superomniphobic responses <sup>40</sup>). Figure 3b illustrates an 8 × 6 array of

overhanging cantilevers mounted on pillars with different heights (also, see Supporting Information Figure S4a). The idea is to demonstrate fine structures composed of re-entrant features, which are responsive to light. This system was polymerized using light filtered with a 495 nm long-pass filter to avoid isomerizing the azobenzene during the polymerization. The pillars have polydomain molecular orientation, and the molecular directors in the monodomain cantilevers are aligned parallel to their long axis, as illustrated in Figure 3b. Cantilevers are 60  $\mu$ m thick and 700  $\mu$ m long. During the sample development to wash off residual monomers after finishing the printing process, the capillary forces from the solvent bent the cantilevers downward. This can be solved by utilizing support structures, which are removed after the development. When this structure is irradiated from the top,

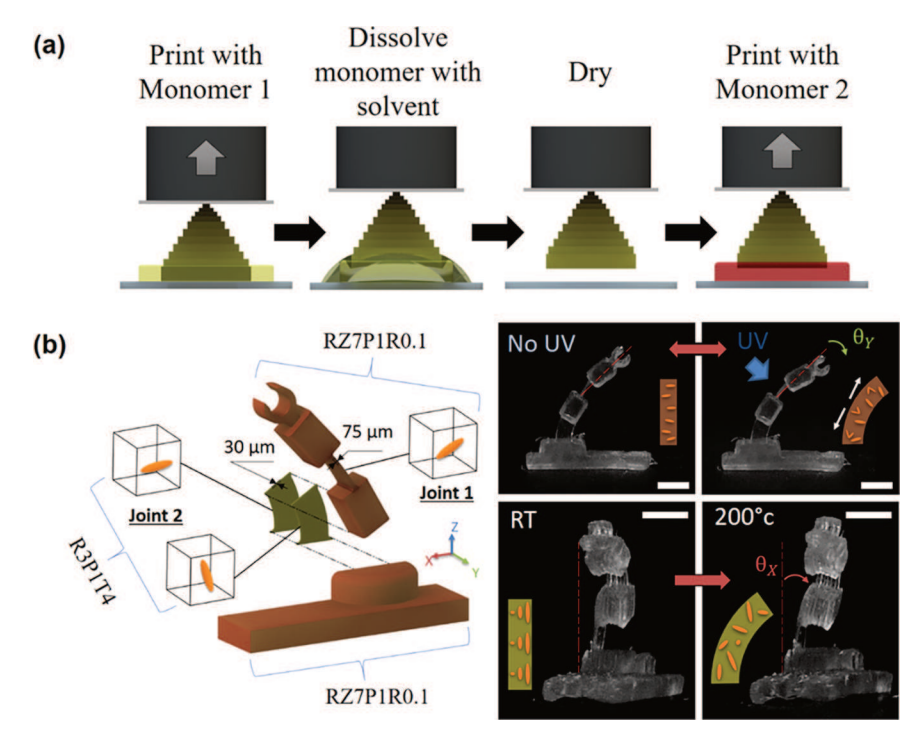


Figure 4. (a) Framework for modulating the composition of the structure between layers. (b) Two-axis robotic arm, which is directly 3D-printed to realize responses to different stimuli in the different joints. The compositions used in the structure are shown. Joint 1 is responsive to light, by bending away from the actinic light due to its molecular pattern. Joint 2 is a bilayered system, which is responsive to heat. Actuation with light ( $\theta_{\nu}$ ) is shown in the top, and the thermal actuation  $(\theta_x)$  is shown in the bottom. Red dashed are used to illustrate the original location of the fingers of the arm (scale bars = 1 mm). Note the different views used in the figure panels to illustrate the multiaxial manipulation in response to different stimuli. Also, see SI Movie 2.

the absorption of light by the overhanging cantilevers leads to their bending toward the light. The deflection is illustrated by tracking the outline of the cantilever, as illustrated in Figure 3b (also, see SI Movie 1). Graded contractile strains ( $\sim$ -1.8% strain on the exposed side) are generated along the nematic director, which generates the bending. Strains were calculated by measuring the change in the curvature of the cantilevers  $(\Delta \kappa)$  and the initial bending angle  $(\alpha)$ . After the UV light was turned off, the cantilever spontaneously relaxed to its initial shape after ~30 min at ambient temperature. The ability to fabricate such responsive microstructures along arbitrary surface profiles can hold the key to modulating functional responses, including hydrophobicity, fluid drag, and biological responses.

The inverted additive manufacturing framework, which involves polymerizing incremental elements of the material in a build gap, allowed for modulating the composition layer by layer to achieve gradations in responses to stimuli. Figure 4a illustrates the approach for creating integral, molecularly ordered structures with multiple materials. Consider printing with monomer 1 (e.g., R3P1T4) to build a structure. Then, a change in the composition is desired to monomer 2 (e.g., RZ7P1R0.1). To accomplish this, after printing with monomer 1, the build plate is retracted to release the sample from the PDMS substrate. After the temperature is lowered to ambient, a solvent (toluene and isopropyl alcohol (IPA) in a 4:1 weight ratio) is introduced to dissolve the residual monomers while not swelling the polymerized structure. Then, the build plate is reset to the desired location, and the temperature is raised to dry the build gap. Now, the second monomer is introduced, and the build process continues.

Using this multicomposition process, a multiresponsive robotic arm was built. Figure 4b illustrates an arm, which is capable of two independent degrees of freedom ( $\theta_v$  and  $\theta_r$ ), which are responsive to light and heat, respectively. The segments of the arm are fabricated using RZ7P1R0.1 without applying a magnetic field (polydomain nematic orientation). They are intentionally bulky to ensure they remain entirely nonresponsive and serve a structural role. Joint 1, which is designed to be light-responsive, is also fabricated using RZ7P1R0.1 and is characterized by a homeotropic alignment through its thin axis over the entire thickness of 75  $\mu$ m. Irradiating this joint with 365 nm light leads to bending away from the actinic source. As seen in the SI Movie 2, irradiating from different sides can be used to drive back and forth actuation at this joint by  $\theta_{\nu} \sim 9^{\circ}$ . Another joint 2 was fabricated with the heat-responsive R3P1T4 monomer mixture in a bilayered configuration, as illustrated in Figure 4b. The slender axis (60  $\mu$ m thickness) of this joint is designed to be normal to that of joint 1 to enable the bending to occur along an orthogonal axis. Heating the entire structure elicits a bending behavior along  $\theta_r \sim 11^\circ$ . This behavior is roughly analogous to that observed in twisted nematic LCP created using an analogous composition in ref 34. In addition to actuating the joints using one stimulus at a time, the combined application of heat and light leads to the simultaneous triggering of manipulation along both  $\theta_v$  and  $\theta_x$ . Further study could assess the development of sequential actuation by fabricating robotic components with different transition temperatures<sup>20</sup> or separate light-responsive units (joints) that can be actuated independently. 41 This work also paves the way for applications such as mechanical logic 42,43 in which each active unit acts as an input and a specific complex route can be programmed by utilizing the embodied AND/OR/NAND logics. This can give rise to the development of feedback loop, adaptability, and autonomy that are the major concepts in developing robots.

### 3. CONCLUSIONS

A framework for voxel-by-voxel indexing of the molecular order in 3D freeforms is realized with magnetically assisted additive manufacturing of liquid crystalline polymers. The underlying idea is to utilize a reorientable magnetic field and spatially resolved irradiation from a digital micromirror device to build 3D objects in an inverted (bottom-up) configuration. We identify monomer compositions, optimized for controlling the polymerization depth and stimulus response, to enable the fabrication of heat or light-responsive structures at scales ranging from the micro- to the macroscale. This platform expands the design space of molecularly ordered solids to enable microstructural and composition gradients in hitherto difficult-to-realize geometries. These include the free-form fabrication of light-responsive topographies, heat-responsive structures that generate Gaussian curvatures from flat geometries, and the creation of multiresponsive robotic manipulators, which can be controlled using heat and/or light. The presented fabrication platform provides the opportunity to expand the application of molecularly ordered materials to soft machines, micromechanical devices that are driven by unconventional stimuli (e.g., light), and smart surfaces capable of tailorable functionalities (e.g., friction, wettability, reflectance).

## 4. METHODS

4.1. Materials. Thermal-responsive resin mixture was created using RM257 (1,4-bis-[4-(3-acryloyloxypropyloxy)benzoyloxy]-2methylbenzene) monomer (Wilshire Technologies) mixed with Irgacure 369 (Ciba Specialty Chemicals) as the photoinitiator, Tinuvin 328: 2-(2H-benzotriazol-2-yl)-4,6-di-tert-pentylphenol (Sigma-Aldrich) as the light absorber, and methylhydroquinone (Sigma-Aldrich) as the inhibitor. A range of compositions illustrated in Table 1 were examined. Light-responsive resin mixtures (Table 2) were created using RM257 monomer mixed with azo 6c (4,4'-di(6-(acryloxy)-hexyloxy)azobenzene), which was synthesized using the procedure described in ref 36, Irgacure 784 (Ciba Specialty Chemicals) as the photoinitiator, and methyl red (2-(4dimethylaminophenylazo)benzoic acid, 4-dimethylaminoazobenzene-2'-carboxylic acid, and acid red 2 purchased from Sigma-Aldrich) as the light absorber. After making the composition, the material was melted and vortexed. It was then dispensed on the PDMS during the layer-by-layer fabrication of the structures. The solvent that was used for removing the monomer during the development of the part at the end of the printing process contained toluene (Fisher Scientific) and isopropanol (Fisher Scientific) with 4:1 wt.

4.2. Fabrication System. A commercially available DMD projector (D912HD, Vivitek), which was modified to remove the UV filters, was proposed for these experiments. The position of the build plate was controlled using a one-axis motorized translation stage (PT1/M—Z8, Thorlabs). The bottom window was made of a clear acrylic sheet coated with a thin layer of PDMS (Sylgard 184 Dow Corning 184 Silicone Elastomer). To control the printing temperature, a heating system including a ring disc heater (200W, McMaster), a temperature controller (PXR3, Fuji Electric), thermocouples (5SRTC-TT-J-30-36, Omega), and a thermometer (HH802U, Omega) was built. Permanent neodymium magnets were purchased from K&J Magnetics and mounted on a motorized rotation stage (PRM1Z8, Thorlabs) to control the direction of the magnetic field.

**4.3. Printing Method.** First, a 3D model of the desired structure was designed using Solidworks (Dassault Systems) and saved in .stl format. Then, the 3D model was sliced into black-and-white 2D patterns of the cross section, using slicer software (CreationWorkshops). These patterns were used later to photopolymerize the cross section at each layer. Within each layer of the structure, regions that have a different molecular alignment were placed in different layers in the CAD model to produce different patterns after the slicing step. A coverslip (build plate) was spin-coated with Elvamide (DuPont) to achieve sufficient adhesion between the cured material and the coverslip. If needed, it can also be rubbed in suitable directions to impose the alignment on mesogens close to the build plate. Once the coverslip was attached to the platform, it was moved to the desired location (build gap) close to the PDMS. The cell was then heated to the desired temperature that falls within the nematic phase range of the monomer. The molten monomer mixture was then introduced into the build gap to build the subsequent layers. A 0.3 T magnetic field was introduced using two neodymium permanent magnets (grade N52, K&J Magnetics). To achieve the programmed orientation induced by the magnetic field, a 5 min dwell time was induced before polymerization. The dwell time provides enough time for the mesogens to rotate and align parallel with the magnetic field. Then, the desired 2D pattern was exposed. The exposure period and intensity were derived from the working curve. For light-responsive materials, a 495 nm long-pass filter was used. The printing process continued by lifting the platform, rotating the magnetic field (if required), and exposing 2D patterns repeatedly. When all of the layers were polymerized and the 3D object was completed, the build plate moved up and the printed structure was removed from the printer. For the final development, the sample was immersed in the solvent (toluene and IPA 4:1) for 2-5 min. Finally, it was dried in a vacuum chamber for 2-3 min. The final product generally required postcuring process, which was executed by exposing ~20 mW cm<sup>-2</sup> UV light (green light for light-responsive materials) for about 30 min or heating the sample up to 75 °C for 1 h.

**4.4. Measurement of Working Curves.** The curing depth was measured for the variety of photonic energy intensities and material compositions in Tables 1 and 2. By controlling the grayscale values in the 2D patterns, which were projected, control over the light intensity was achieved. Direct measurements of intensity using a power meter were performed. To measure the polymerization depth, the build plate was placed ~2 mm from the PDMS and the whole gap was filled with the monomer. By exposing square patterns with different intensities, the polymerization started from the PDMS surface up to some level below the build plate. Squares with higher intensity (brighter patterns) cured up to higher levels. Measuring the thickness of these squares by a digital micrometer yielded polymerization depth for the respected conditions. This data was used to populate the working curves, which are illustrated in Figure 2a,b.

## ASSOCIATED CONTENT

#### S Supporting Information

The Supporting Information is available free of charge on the ACS Publications website at DOI: 10.1021/acsami.9b04480.

3D printer setup and its components, 2D patterns, and actuation of basket-like geometries (PDF)

Light actuation of overhanging cantilevers (AVI)

Irradiating UV light from different sides to drive the robotic arm back and forth (AVI)

#### AUTHOR INFORMATION

## **Corresponding Author**

\*E-mail: ravishm@pitt.edu.

ORCID

Mohsen Tabrizi: 0000-0003-1953-673X Taylor H. Ware: 0000-0001-7996-7393

### **Author Contributions**

M.T., T.H.W., and M.R.S. conceived the research. M.T. composed the manuscript. M.R.S. oversaw the preparation of the manuscript. All authors reviewed the manuscript.

#### **Notes**

The authors declare no competing financial interest.

### ACKNOWLEDGMENTS

Support from the Office of Naval Research (N00014-18-1-2856) and the National Science Foundation (1727551, 1728181, and 1752846) are gratefully acknowledged.

### REFERENCES

- (1) Wehner, M.; Truby, R. L.; Fitzgerald, D. J.; Mosadegh, B.; Whitesides, G. M.; Lewis, J. A.; Wood, R. J. An Integrated Design and Fabrication Strategy for Entirely Soft, Autonomous Robots. *Nature* **2016**, *536*, 451–455.
- (2) Chen, T.; Bilal, O. R.; Shea, K.; Daraio, C. Harnessing Bistability for Directional Propulsion of Untethered, Soft Robots. *Proc. Natl. Acad. Sci.* **2018**, *115*, 5698–5702.
- (3) Kim, Y.; Yuk, H.; Zhao, R. K.; Chester, S. A.; Zhao, X. H. Printing Ferromagnetic Domains for Untethered Fast-Transforming Soft Materials. *Nature* **2018**, *558*, 274–279.
- (4) Gladman, A. S.; Matsumoto, E. A.; Nuzzo, R. G.; Mahadevan, L.; Lewis, J. A. Biomimetic 4D Printing. *Nat. Mater.* **2016**, *15*, 413–418.
- (5) Ware, T. H.; White, T. J. Programmed Liquid Crystal Elastomers with Tunable Actuation Strain. *Polym. Chem.* **2015**, *6*, 4835–4844.
- (6) Küpfer, J.; Finkelmann, H. Nematic Liquid Single Crystal Elastomers. *Makromol. Chem., Rapid Commun.* 1991, 12, 717–726.
- (7) Kim, H.; Boothby, J. M.; Ramachandran, S.; Lee, C. D.; Ware, T. H. Tough, Shape-Changing Materials: Crystallized Liquid Crystal Elastomers. *Macromolecules* **2017**, *50*, 4267–4275.
- (8) Harris, K. D.; Bastiaansen, C. W. M.; Broer, D. J. Physical Properties of Anisotropically Swelling Hydrogen-Bonded Liquid Crystal Polymer Actuators. *J. Microelectromech. Syst.* **2007**, *16*, 480–488.
- (9) White, T. J.; Broer, D. J. Programmable and Adaptive Mechanics with Liquid Crystal Polymer Networks and Elastomers. *Nat. Mater.* **2015**, *14*, 1087–1098.
- (10) Warner, M.; Terentjev, E. M. Liquid Crystal Elastomers; Oxford university press: 2007; Vol. 120.
- (11) van Oosten, C. L.; Bastiaansen, C. W. M.; Broer, D. J. Printed Artificial Cilia from Liquid-Crystal Network Actuators Modularly Driven by Light. *Nat. Mater.* **2009**, *8*, 677–682.
- (12) Hendrikx, M.; Sırma, B.; Schenning, A. P. H. J.; Liu, D. Q.; Broer, D. J. Compliance-Mediated Topographic Oscillation of Polarized Light Triggered Liquid Crystal Coating. *Adv. Mater. Interfaces* **2018**, *5*, No. 1800810.
- (13) Ware, T. H.; McConney, M. E.; Wie, J. J.; Tondiglia, V. P.; White, T. J. Voxelated Liquid Crystal Elastomers. *Science* **2015**, 347, 982–984.
- (14) Schuhladen, S.; Preller, F.; Rix, R.; Petsch, S.; Zentel, R.; Zappe, H. Iris-like Tunable Aperture Employing Liquid-Crystal Elastomers. *Adv. Mater.* **2014**, *26*, 7247–7251.
- (15) Yao, Y. X.; Waters, J. T.; Shneidman, A. V.; Cui, J. X.; Wang, X. G.; Mandsberg, N. K.; Li, S. C.; Balazs, A. C.; Aizenberg, J. Multiresponsive Polymeric Microstructures with Encoded Predetermined and Self-Regulated Deformability. *Proc. Natl. Acad. Sci. U.S.A.* **2018**, *115*, 12950–12955.
- (16) Ambulo, C. P.; Burroughs, J. J.; Boothby, J. M.; Kim, H.; Shankar, M. R.; Ware, T. H. Four-Dimensional Printing of Liquid Crystal Elastomers. *ACS Appl. Mater. Interfaces* **2017**, *9*, 37332–37339.
- (17) Kotikian, A.; Truby, R. L.; Boley, J. W.; White, T. J.; Lewis, J. A. 3D Printing of Liquid Crystal Elastomeric Actuators with Spatially Programed Nematic Order. *Adv. Mater.* **2018**, *30*, No. 1706164.

- (18) López-Valdeolivas, M.; Liu, D.; Broer, D. J.; Sánchez-Somolinos, C. 4D Printed Actuators with Soft-Robotic Functions. *Macromol. Rapid Commun.* **2018**, 39, No. 1700710.
- (19) Gantenbein, S.; Masania, K.; Woigk, W.; Sesseg, J. P. W.; Tervoort, T. A.; Studart, A. R. Three-Dimensional Printing of Hierarchical Liquid-Crystal-Polymer Structures. *Nature* **2018**, *561*, 226–230.
- (20) Saed, M. O.; Ambulo, C. P.; Kim, H.; De, R.; Raval, V.; Searles, K.; Siddiqui, D. A.; Cue, J. M. O.; Stefan, M. C.; Shankar, M. R.; et al. Molecularly-Engineered, 4D-Printed Liquid Crystal Elastomer Actuators. *Adv. Funct. Mater.* **2019**, 29, No. 1806412.
- (21) Roach, D. J.; Kuang, X.; Yuan, C.; Chen, K.; Qi, H. J. Novel Ink for Ambient Condition Printing of Liquid Crystal Elastomers for 4D Printing. *Smart Mater. Struct.* **2018**, 27, No. 125011.
- (22) Mostajeran, C.; Warner, M.; Ware, T. H.; White, T. J. Encoding Gaussian Curvature in Glassy and Elastomeric Liquid Crystal Solids. *Proc. R. Soc. A* **2016**, 472, No. 20160112.
- (23) Guin, T.; Settle, M. J.; Kowalski, B. A.; Auguste, A. D.; Beblo, R. V.; Reich, G. W.; White, T. J. Layered Liquid Crystal Elastomer Actuators. *Nat. Commun.* **2018**, *9*, No. 2531.
- (24) Zeng, H.; Martella, D.; Wasylczyk, P.; Cerretti, G.; Lavocat, J.-C. G.; Ho, C.-H.; Parmeggiani, C.; Wiersma, D. S. High-Resolution 3d Direct Laser Writing for Liquid-Crystalline Elastomer Microstructures. *Adv. Mater.* **2014**, *26*, 2319–2322.
- (25) Zeng, H.; Wasylczyk, P.; Parmeggiani, C.; Martella, D.; Burresi, M.; Wiersma, D. S. Light-Fueled Microscopic Walkers. *Adv. Mater.* **2015**, *27*, 3883–3887.
- (26) Boothby, J. M.; Kim, H.; Ware, T. H. Shape Changes in Chemoresponsive Liquid Crystal Elastomers. *Sens. Actuators, B* **2017**, 240, 511–518.
- (27) Ware, T. H.; Perry, Z. P.; Middleton, C. M.; Iacono, S. T.; White, T. J. Programmable Liquid Crystal Elastomers Prepared by Thiol–Ene Photopolymerization. *ACS Macro Lett.* **2015**, *4*, 942–946.
- (28) Shankar, M. R.; Smith, M. L.; Tondiglia, V. P.; Lee, K. M.; McConney, M. E.; Wang, D. H.; Tan, L.-S.; White, T. J. Contactless, Photoinitiated Snap-through in Azobenzene-Functionalized Polymers. *Proc. Natl. Acad. Sci.* **2013**, *110*, 18792–18797.
- (29) Coleman, B. D.; Swigon, D. Theory of Supercoiled Elastic Rings with Self-Contact and Its Application to DNA Plasmids. *J. Elast. Phys. Sci. solids* **2000**, *60*, 173.
- (30) Gent, A. N.; Hua, K.-C. Torsional Instability of Stretched Rubber Cylinders. *Int. J. Nonlinear Mech.* **2004**, *39*, 483–489.
- (31) Norman, A. D.; Seffen, K. A.; Guest, S. D. Morphing of Curved Corrugated Shells. *Int. J. Solids Struct.* **2009**, *46*, 1624–1633.
- (32) Prost, J.; Gennes, P. G. The Physics of Liquid Crystals; Oxford university press: 1995; Vol. 83.
- (33) Iizuka, E. The Effects of Magnetic Fields on the Structure of Cholesteric Liquid Crystals of Polypeptides. *Polym. J.* 1973, 4, 401–
- (34) Lee, K. M.; Bunning, T. J.; White, T. J. Autonomous, Hands-Free Shape Memory in Glassy, Liquid Crystalline Polymer Networks. *Adv. Mater.* **2012**, *24*, 2839–2843.
- (35) Jacobs, P. F. Rapid Prototyping & Manufacturing: Fundamentals of Stereolithography; Society of Manufacturing Engineers, 1992.
- (36) Skandani, A.; Clement, J. A.; Tristram-Nagle, S.; Shankar, M. R. Aliphatic Flexible Spacer Length Controls Photomechanical Response in Compact, Ordered Liquid Crystalline Polymer Networks. *Polymer* **2017**, *133*, 30–39.
- (37) Yu, Y. L.; Nakano, M.; Shishido, A.; Shiono, T.; Ikeda, T. Effect of Cross-Linking Density on Photoinduced Bending Behavior of Oriented Liquid-Crystalline Network Films Containing Azobenzene. *Chem. Mater.* **2004**, *16*, 1637–1643.
- (38) Mouthuy, P.-O.; Coulombier, M.; Pardoen, T.; Raskin, J. P.; Jonas, A. M. Overcurvature Describes the Buckling and Folding of Rings from Curved Origami to Foldable Tents. *Nat. Commun.* **2012**, 3, No. 1290.
- (39) Yu, Y. L.; Nakano, M.; Ikeda, T. Photomechanics: Directed Bending of a Polymer Film by Light. *Nature* **2003**, *425*, 145.

- (40) Choi, J.; Jo, W.; Lee, S. Y.; Jung, Y. S.; Kim, S.-H.; Kim, H.-T. Flexible and Robust Superomniphobic Surfaces Created by Localized Photofluidization of Azopolymer Pillars. *ACS Nano* **2017**, *11*, 7821–7828
- (41) Palagi, S.; Mark, A. G.; Reigh, S. Y.; Melde, K.; Qiu, T.; Zeng, H.; Parmeggiani, C.; Martella, D.; Sanchez-Castillo, A.; Kapernaum, N.; et al. Structured Light Enables Biomimetic Swimming and Versatile Locomotion of Photoresponsive Soft Microrobots. *Nat. Mater.* **2016**, *15*, 647–653.
- (42) Jiang, Y.; Korpas, L. M.; Raney, J. R. Bifurcation-Based Embodied Logic and Autonomous Actuation. *Nat. Commun.* **2019**, *10*. No. 128.
- (43) Jeong, H. Y.; Lee, E.; Ha, S.; Kim, N.; Jun, Y. C. Multistable Thermal Actuators Via Multimaterial 4D Printing. *Adv. Mater. Technol.* **2019**, *4*, No. 1800495.